

Interfaces: Adsorption, Reactions, Films, Forces, Measurement Techniques, Charge Transfer, Electrochemistry, Electrocatalysis, Energy Production and Storage

On the Adsorption of DNA Origami Nanostructures in Nanohole Arrays

Katharina Brassat, Saminathan Ramakrishnan, Julius Bürger, Marcel Hanke,
Mahnaz Doostdar, Jörg K. N. Lindner, Guido Grundmeier, and Adrian Keller

Langmuir, **Just Accepted Manuscript** • DOI: 10.1021/acs.langmuir.8b00793 • Publication Date (Web): 13 May 2018

Downloaded from <http://pubs.acs.org> on May 22, 2018

Just Accepted

“Just Accepted” manuscripts have been peer-reviewed and accepted for publication. They are posted online prior to technical editing, formatting for publication and author proofing. The American Chemical Society provides “Just Accepted” as a service to the research community to expedite the dissemination of scientific material as soon as possible after acceptance. “Just Accepted” manuscripts appear in full in PDF format accompanied by an HTML abstract. “Just Accepted” manuscripts have been fully peer reviewed, but should not be considered the official version of record. They are citable by the Digital Object Identifier (DOI®). “Just Accepted” is an optional service offered to authors. Therefore, the “Just Accepted” Web site may not include all articles that will be published in the journal. After a manuscript is technically edited and formatted, it will be removed from the “Just Accepted” Web site and published as an ASAP article. Note that technical editing may introduce minor changes to the manuscript text and/or graphics which could affect content, and all legal disclaimers and ethical guidelines that apply to the journal pertain. ACS cannot be held responsible for errors or consequences arising from the use of information contained in these “Just Accepted” manuscripts.



On the Adsorption of DNA Origami Nanostructures in Nanohole Arrays

Katharina Brassat,^{#,†,‡} Saminathan Ramakrishnan,^{#,§} Julius Bürger,^{†,‡} Marcel Hanke,[§] Mahnaz Doostdar,[§] Jörg K. N. Lindner,^{†,‡} Guido Grundmeier,[§] and Adrian Keller^{,§}*

[†] Department of Physics, Paderborn University, Warburger Str. 100, 33098 Paderborn, Germany.

[‡] Center for Optoelectronics and Photonics Paderborn CeOPP, Warburger Str. 100, 33098 Paderborn, Germany.

[§] Technical and Macromolecular Chemistry, Paderborn University, Warburger Str. 100, 33098 Paderborn, Germany.

KEYWORDS: DNA origami, directed adsorption, nanosphere lithography, self-assembly, nanohole arrays

ABSTRACT

DNA origami nanostructures are versatile substrates for the controlled arrangement of molecular capture sites with nanometer precision and thus have many promising applications in single-molecule bioanalysis. Here, we investigate the adsorption of DNA origami nanostructures in nanohole arrays which represent an important class of biosensors and may benefit from the incorporation of DNA origami-based molecular probes. Nanoholes with well-defined diameter that enable the adsorption of single DNA origami triangles are fabricated in Au films on Si

1
2
3 wafers by nanosphere lithography. The efficiency of directed DNA origami adsorption on the
4 exposed SiO₂ areas at the bottoms of the nanoholes is evaluated in dependence of various
5 parameters, *i.e.*, Mg²⁺ and DNA origami concentrations, buffer strength, adsorption time, and
6 nanohole diameter. We observe that the buffer strength has a surprisingly strong effect on DNA
7 origami adsorption in the nanoholes and that multiple DNA origami triangles with 120 nm edge
8 length can adsorb in nanoholes as small as 120 nm in diameter. We attribute the latter
9 observation to the low lateral mobility of once adsorbed DNA origami on the SiO₂ surface, in
10 combination with parasitic adsorption to the Au film. While parasitic adsorption can be
11 suppressed by modifying the Au film with a hydrophobic self-assembled monolayer, the limited
12 surface mobility of the adsorbed DNA origami still leads to poor localization accuracy in the
13 nanoholes and results in many DNA origami crossing the boundary to the Au film even under
14 optimized conditions. We discuss possible ways to minimize this effect by varying the
15 composition of the adsorption buffer, employing different fabrication conditions, or using other
16 substrate materials for nanohole array fabrication.

37 38 **INTRODUCTION**

39
40 Since its introduction by Rothemund in 2006,¹ the DNA origami technique with its remarkable
41 versatility and ability to manufacture well-defined 2D and 3D nanoscale objects of almost
42 arbitrary shape has become a wide spread method routinely employed in many labs around the
43 world.² DNA origami nanostructures are assembled by folding a long, single-stranded DNA
44 scaffold into a pre-designed shape via hybridization with about 200 synthetic staple strands, each
45 of which can be unambiguously identified in the assembled DNA origami construct via its
46 unique nucleotide sequence. Therefore, DNA origami nanostructures can be site-selectively
47
48
49
50
51
52
53
54
55
56
57
58
59
60

1
2
3 decorated with functional entities such as reactive chemical groups,³ fluorophores,⁴ proteins,⁵
4 DNA topologies,⁶ metallic nanoparticles,⁷ and semiconductor quantum dots⁸ by incorporation of
5 modified staple strands at selected positions. This great versatility has resulted in a broad range
6 of applications that exploit the unprecedented structural control provided by the DNA origami
7 technique. Functionalized DNA origami have for instance been utilized as substrates for single-
8 molecule studies,^{3,9} as drug delivery vehicles,^{10,11} biosensors,^{12,13} and SERS substrates,^{14,15} as
9 masks for molecular lithography,^{16,17} and as templates for the fabrication of electronic,^{18,19}
10 plasmonic,^{20,21} and photonic nanostructures.^{22,23}

11
12
13
14
15
16
17
18
19
20
21
22 Many of the technological applications of DNA origami nanostructures critically rely on their
23 precise placement on a substrate surface. Consequently, a large number of previous studies have
24 evaluated various methods for the controlled immobilization and/or alignment of DNA origami
25 nanostructures on different application-relevant materials.^{24–34} Most of the approaches reported
26 in literature have employed top-down photo- or electron beam lithography to fabricate
27 prepatterned substrate surfaces to direct DNA origami adsorption to chemically different micro-
28 or nanoscale patches.^{24–30} Other studies have utilized receding menisci for the manipulation of
29 already adsorbed DNA origami,^{31,32} or self-organized nanopatterns for the selective adsorption of
30 DNA origami nanostructures.^{33,34}

31
32
33
34
35
36
37
38
39
40
41
42
43 In this work, we investigate directed DNA origami adsorption in nanohole arrays patterned into
44 thin Au films on Si wafers by nanosphere lithography (NSL). NSL is a technique based on self-
45 organization that enables the large-area patterning of surfaces with nanoscale features.³⁵ To this
46 end, (mono-) layers of nanospheres are assembled on solid surfaces by convective self-assembly
47 of colloidal nanospheres from suspensions.^{36,37} Evaporation fluxes of the liquid medium of the
48 suspension lead to an increased nanosphere concentration at a forming triple phase boundary
49
50
51
52
53
54
55
56
57
58
59
60

1
2
3 between the liquid suspension, the solid substrate, and the surrounding gas phase. Along this
4 triple phase boundary, capillary forces act on the nanospheres and draw them together, resulting
5 in hexagonally close-packed nanosphere arrangements. In NSL, such nanosphere layers are used
6 as a shadow mask in a subsequent deposition step³⁵ during which material is deposited onto the
7 nanospheres as well as onto the substrate through the mask openings in the nanosphere layer.
8
9

10
11
12
13
14
15 NSL enables the fabrication of various and often surprisingly complex patterns over large
16 surface areas,^{38,39} which are for instance frequently used in protein patterning.³⁹⁻⁴¹ On the other
17 hand, NSL-fabricated nanohole arrays in Au films exhibit unique plasmonic properties^{42,43} and
18 are thus used extensively in biosensing and on-chip bioanalysis.^{44,45} Immobilizing DNA origami
19 nanostructures inside individual nanoholes may enable the introduction of single molecular
20 capture sites and thereby provide additional benefits with regard to target specificity and
21 sensitivity.⁴⁶ While the specific adsorption of single biotin-carrying DNA origami nanostructures
22 inside similar nanoholes has already been demonstrated using neutravidin-modified substrate
23 surfaces,⁴⁶ we here study non-specific DNA origami adsorption to the exposed SiO₂ surface at
24 the bottom of the nanoholes in a Au film. In particular, we investigate the effect of buffer
25 conditions on directed DNA origami adsorption in the nanohole arrays. We find that the strength
26 of the adsorption buffer has a surprisingly strong influence and that the low surface mobility of
27 once-adsorbed DNA origami is negatively affecting adsorption selectivity and positioning
28 accuracy even under optimized conditions.
29
30
31
32
33
34
35
36
37
38
39
40
41
42
43
44
45
46

47 **MATERIALS AND METHODS**

48 **Nanosphere lithography.**

49
50
51
52
53 Epi-polished Si(100) wafers with native surface oxide were cleaned in a plasma of 2 sccm O₂
54 and 8 sccm Ar at a pressure of 75 mTorr and 50 W RF power for 5 minutes (Plasma Technology
55
56
57
58
59
60

1
2
3 Plasma Lab u80p). 7 μl droplets of an aqueous suspension of polystyrene (PS) nanospheres with
4 a diameter of 202 nm ($< 3\%$ coefficient of variance (CV), 5 % w/v solid content, Microparticles
5 GmbH) were deposited onto the cleaned Si surfaces at a substrate temperature of 30°C. The
6 droplet was driven across the Si surface with a hydrophobic blade at a constant velocity of 100
7 $\mu\text{m/s}$, resulting in the formation of a hexagonally close-packed nanosphere monolayer due to
8 controlled solvent evaporation and capillary forces acting between the PS nanospheres.
9

10
11
12 The assembled PS nanospheres were exposed to an O_2/Ar plasma with the same parameters as
13 reported above in order to remove part of the PS and shrink the nanospheres in diameter while
14 maintaining their position on the substrate.⁴⁷ The final diameter can be controlled by the duration
15 of the plasma treatment:⁴⁸ here, a treatment for 45 sec was used to reduce the nanosphere
16 diameter from 202 nm to 160 nm; after 90 sec the diameter reaches 120 nm.
17

18
19
20 10 nm Au were deposited onto the samples by electron beam evaporation. To ensure conformal
21 growth of the Au film, 2 nm Ti were deposited prior to Au as adhesion promoter without
22 breaking the vacuum (base pressure 5×10^{-6} mbar) between deposition steps. After deposition,
23 the nanospheres were removed by chemical dissolution in tetrahydrofuran (Carl Roth) in an
24 ultrasonic bath. Carbon residues from the PS nanospheres which remained on the Si surface after
25 ultrasonication were removed by dipping the samples into a 10 % aq. HF (Carl Roth) solution for
26 5 seconds. This harsh cleaning procedure was necessary since alternative treatments were not
27 able to remove all the carbon residues (see figure S1).
28

29 **Scanning electron microscopy (SEM).**

30
31
32 SEM images were taken with a Raith Pioneer at an acceleration voltage of 5 kV using the in-lens
33 detector. Image analysis was performed with a home-made software. The nanohole diameters
34
35
36
37
38
39
40
41
42
43
44
45
46
47
48
49
50

1
2
3 were evaluated by a grey-scale thresholding technique, the density and coordination by a
4
5 Delaunay triangulation-based algorithm.
6

7 8 **DNA origami assembly.** 9

10
11 DNA origami triangles¹ were synthesized as described previously,¹⁶ using the M13mp18 scaffold
12
13 (Tilibit) and 208 staple strands (Metabion). Assembly was performed in 1x TAE (Carl Roth)
14
15 with 10 mM MgCl₂ (Sigma-Aldrich) by stepwise thermal annealing in a thermocycler Primus 25
16
17 advanced (PEQLAB). Excess staples were removed after assembly by spin filtering using 100
18
19 kDa MWCO filters (Amicon Ultra, Millipore). After filtering, the DNA origami concentration
20
21 was measured by UV/Vis absorption with an Implen Nanophotometer P330.
22
23
24

25 26 **DNA origami adsorption.** 27

28
29 The nanohole array substrates were first cleaned with ethanol and water. A mild oxygen plasma
30
31 cleaning (Zepto, Diener electronic) was carried out for 1 min with 50 % power before DNA
32
33 origami adsorption. For DNA origami adsorption, 1x TAE and 2.5x TAE stock solutions were
34
35 prepared with 10 mM MgCl₂. For the higher MgCl₂ concentration of 50 mM, working solutions
36
37 were freshly prepared by adding the required volume from a 1 M MgCl₂ stock solution. All
38
39 buffer solutions had a pH of 8.5. The DNA origami sample was then diluted in the respective
40
41 buffer solutions to the desired concentrations. The nanohole array substrate was placed on a
42
43 stage inside a humidity chamber to avoid evaporation and 100 µl of the resulting sample solution
44
45 were slowly dropped on the surface. After incubation, the sample was carefully washed with 4
46
47 ml of HPLC-grade water (VWR) and dried in a stream of ultrapure air.
48
49
50

51 52 **Self-assembled monolayer (SAM) fabrication.** 53 54 55 56 57 58 59 60

1
2
3 Plasma-cleaned nanohole array samples were immersed in 1 mM 1-octadecanethiol (ODT,
4 Sigma-Aldrich) in ethanol for 24 h to form hydrophobic SAMs on the surfaces of the Au films.
5
6 Immediately before the adsorption experiments, the SAM-coated nanohole arrays were rinsed
7
8 with ethanol and dried in a stream of ultrapure air. The ODT SAMs formed under these
9
10 conditions exhibit high packing densities and render the Au surface fully hydrophobic.⁴⁹
11
12
13

14 15 **Atomic force microscopy (AFM).** 16

17
18 The samples were imaged in intermittent contact mode in air using an Agilent 5100 AFM and
19
20 HQ: NSC18/Al BS cantilevers (MikroMasch). Yields are presented as averages over three AFM
21
22 images taken at different positions on the sample surface with standard deviations as error bars.
23
24 A minimum 600 individual nanoholes were analyzed for each condition.
25
26
27

28 **RESULTS AND DISCUSSION** 29

30
31 The experimental strategy is schematically summarized in figure 1. Ordered nanohole arrays are
32
33 fabricated by NSL. To this end, hexagonally close-packed monolayers of PS nanospheres are
34
35 assembled on a Si wafer by convective self-assembly using the doctor blade technique.⁵⁰ The
36
37 assembled PS nanospheres are then shrunk by exposure to an O₂/Ar plasma to create an array of
38
39 well-separated yet hexagonally ordered nanospheres. The shrunk nanospheres then act as a
40
41 shadow mask for physical vapor deposition. A 10 nm thin Au film is deposited onto the sample,
42
43 *i.e.*, the shrunk nanospheres and bare SiO₂ in the gaps between the nanospheres. Lift-off of the
44
45 nanospheres by dissolution uncovers the final surface pattern, *i.e.*, a thin Au film exhibiting
46
47 hexagonally arranged nanoholes which expose the untreated SiO₂ surface at their bottoms. These
48
49 confined SiO₂ surfaces at the bottoms of the nanoholes are then used to direct DNA origami
50
51 adsorption.
52
53
54
55
56
57
58
59
60

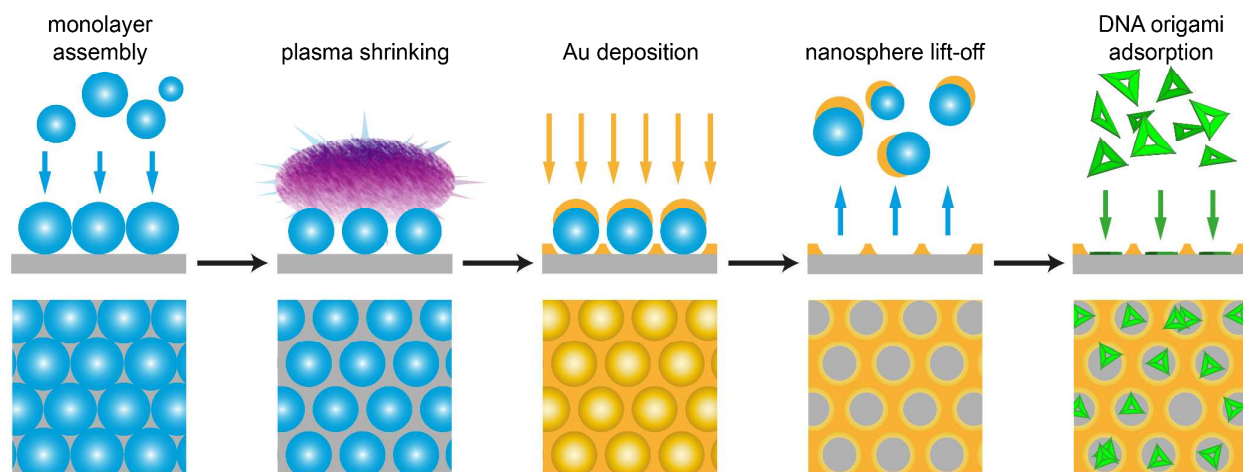
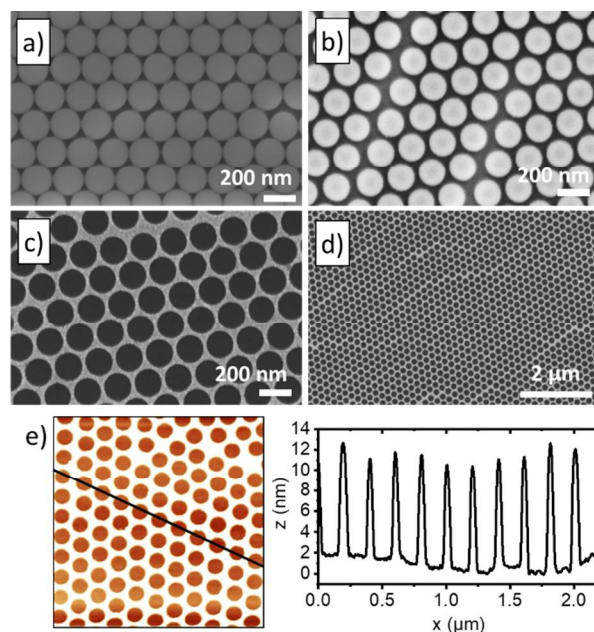


Figure 1. Experimental strategy: A hexagonally ordered pattern of nanoholes in a thin Au film on a Si wafer is fabricated by NSL and used to direct the adsorption of DNA origami nanostructures.

The fabricated nanohole patterns are characterized in figure 2. Analysis of the SEM images reveals a diameter of the nanoholes of 160 ± 16 nm and a nanohole density of 2.6×10^9 cm⁻² over substrate areas of several cm². In addition, 95 % of the nanoholes show perfect sixfold coordination with < 2 % of defects occurring due to dislocation lines or grain boundaries and approximately 3 % point defects. The AFM height profile shown in figure 2e reveals a thickness of the Ti/Au film between 10 and 12 nm, in good agreement with the nominal thicknesses deposited of 2 nm Ti and 10 nm Au. The optical properties of these nanohole arrays are characterized in figure S2. The nanohole diameter of 160 nm allows for adsorbing single triangular DNA origami nanostructures with an edge length of about 120 nm. Due to the lateral confinement of the exposed SiO₂ area by the surrounding Au film, adsorption of more than one DNA origami triangle per nanohole should be restricted. However, since adsorption of the negatively charged DNA origami nanostructures to the negatively charged SiO₂ patches requires divalent cations such as Mg²⁺ in order to form salt bridges between DNA and surface, adsorption

1
2
3 efficiency and especially selectivity can be expected to critically depend on buffer conditions.³²
4
5 Therefore, we have first evaluated the role of Mg^{2+} concentration and buffer strength on DNA
6 origami adsorption in the nanoholes.
7
8
9



10
11
12
13
14
15
16
17
18
19
20
21
22
23
24
25
26
27
28
29
30
31
32 **Figure 2.** *a-d) SEM images of the assembled nanosphere monolayers before (a) and after (b)*
33 *plasma shrinking, and the resulting nanohole array (c,d). e) AFM image of the nanohole array*
34 *and corresponding height profile taken along the black line indicated in the AFM image.*
35
36
37
38

39 Figure 3a shows AFM images of nanohole patterns after adsorption of 1 nM DNA origami
40 triangles in different buffers for 1 h. Obviously, both buffer strength and Mg^{2+} concentration
41 have significant effects on DNA origami adsorption. Increasing the $MgCl_2$ concentration from 10
42 to 50 mM in 1x TAE results in significantly higher DNA origami coverage of the exposed SiO_2
43 areas. In particular, as the statistical analysis in figure 3a reveals, the fraction of empty nanoholes
44 decreases from more than 70 % at 10 mM $MgCl_2$ to only about 10 % in 50 mM $MgCl_2$.
45
46 Surprisingly, however, this results in only about 40 % of the nanoholes being occupied by a
47 single DNA origami, whereas half of the nanoholes exhibit two or even three DNA origami
48
49
50
51
52
53
54
55
56
57
58
59
60

1
2
3 nanostructures. Considering the nominal edge length of the triangles and the average diameter of
4 the nanoholes of 120 nm and 160 nm, respectively, this double and triple occupation can result
5 from two or three DNA origami triangles stacking on top of each other or from only partial
6 adsorption of one or more DNA origami triangles inside the nanoholes with a part of the triangle
7 crossing the boundary to the Au film. Upon closer inspection, examples of both mechanisms can
8 be observed on one sample surface (see figure 3b). However, a statistical analysis reveals that
9 partial adsorption of DNA origami nanostructures accounts for about 63 % of multiply-occupied
10 nanoholes, while only 37 % show vertical stacking. Note that partial adsorption is also frequently
11 observed for singly-occupied nanoholes (see figure 3b, panel 3).
12
13
14
15
16
17
18
19
20
21
22
23
24
25
26
27
28
29
30
31
32
33
34
35
36
37
38
39
40
41
42
43
44
45
46
47
48
49
50
51
52
53
54
55
56
57
58
59
60

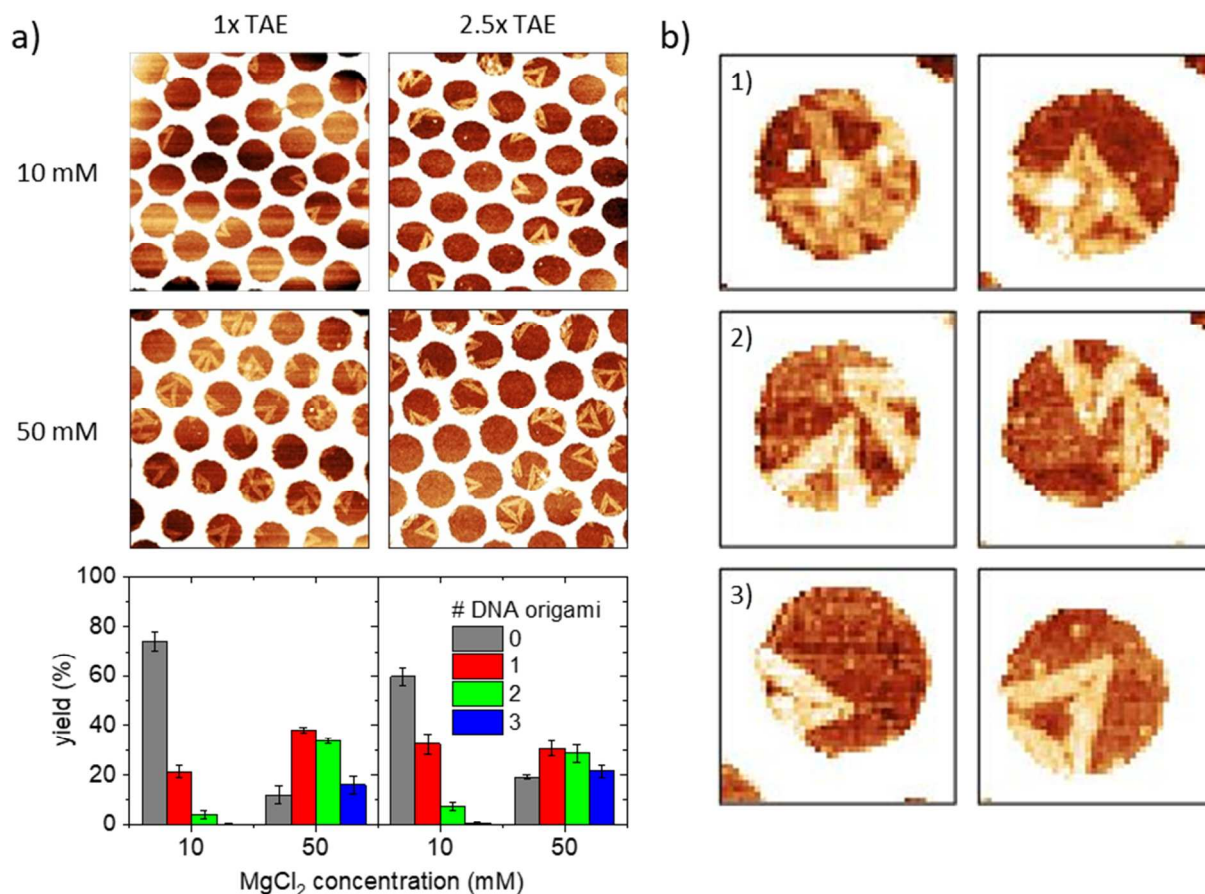


Figure 3. a) AFM images ($1 \times 1 \mu\text{m}^2$, height scales 3 nm) and corresponding statistical analyses of DNA origami triangles adsorbed in the nanohole arrays for two buffer strengths and two MgCl_2 concentrations. The DNA origami concentration was 1 nM and the incubation time 1 h. b) Zoomed AFM images of 1) multiple DNA origami nanostructures adsorbed in single nanoholes via vertical stacking, 2) multiple DNA origami nanostructures adsorbed in single nanoholes via partial adsorption, and 3) single DNA origami nanostructures adsorbed in single nanoholes via partial adsorption. The DNA origami concentration was 1 nM in 1x TAE with 50 mM MgCl_2 and the incubation time 1 h.

Increasing the buffer strength to 2.5x TAE at a constant MgCl_2 concentration of 10 mM results also in a decrease in the fraction of empty nanoholes and a moderate increase in the fraction of

1
2
3 nanoholes occupied by a single DNA origami triangle to about 30 % (see figure 3). However, the
4 fraction of higher occupancies remains below 10 %. Increasing the MgCl_2 concentration to 50
5 mM again leads to a further decrease in the fraction of empty nanoholes which, however, is not
6 as strong as in the case of 1x TAE. This is also reflected in the fraction of singly-occupied
7 nanoholes which remains rather constant. These results demonstrate the non-trivial interplay of
8 buffer strength and Mg^{2+} concentration in DNA origami adsorption to SiO_2 surfaces. Due to the
9 large fraction of nanoholes occupied by more than a single DNA origami triangle at high MgCl_2
10 concentrations, we have used the lower concentration of 10 mM in all the following experiments.

11
12
13
14
15
16
17
18
19
20
21
22 Apart from the buffer conditions, also the DNA origami concentration will affect surface
23 coverage and thereby the occupation of the nanoholes. The effect of DNA origami concentration
24 is therefore evaluated in figure 4, again for two different buffer strengths. Surprisingly,
25 increasing the DNA origami concentration in 1x TAE from 1 nM to 5 nM does not result in any
26 noticeable increase in the DNA origami density. In particular, the fraction of empty and singly-
27 occupied nanoholes remains at about 70 % and about 25 %, respectively, independent of DNA
28 origami concentration.
29
30
31
32
33
34
35
36
37
38
39
40
41
42
43
44
45
46
47
48
49
50
51
52
53
54
55
56
57
58
59
60

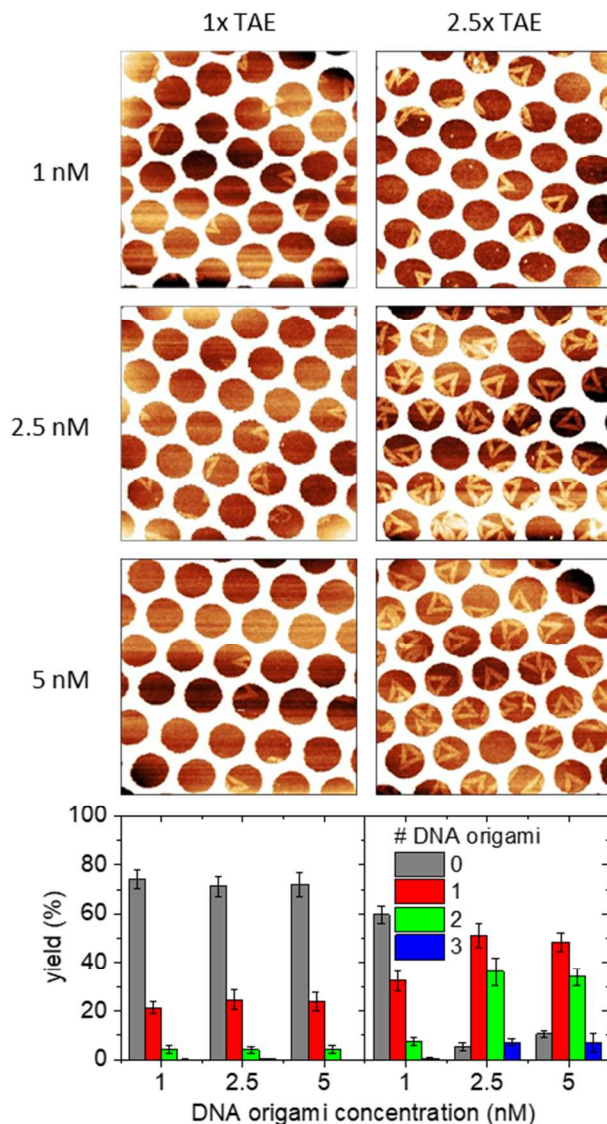


Figure 4. AFM images ($1 \times 1 \mu\text{m}^2$, height scales 3 nm) and corresponding statistical analyses of DNA origami triangles adsorbed in the nanohole arrays for two buffer strengths and three DNA origami concentrations. The MgCl_2 concentration was 10 mM and the incubation time 1 h.

At the higher buffer strength of 2.5x, the situation is notably different. As can be seen in figure 4, increasing the DNA origami concentration from 1 nM to 2.5 nM results in a drastic decrease in the fraction of empty nanoholes from about 60 % to roughly 10 %. At the same time, the fraction of nanoholes occupied by a single DNA origami triangle increases from about 30 % to about 50

1
2
3 % . At this DNA origami concentration, the second most dominant population is represented by
4
5 nanoholes occupied by two DNA origami triangles at about 35 %. Further increase of the DNA
6
7 origami concentration to 5 nM, however, does not result in any significant changes in these
8
9 numbers.
10

11
12 Finally, we set out to investigate the influence of adsorption time on directed DNA origami
13
14 adsorption in the nanohole arrays. For these experiments, we used a DNA origami concentration
15
16 of 1 nM since this concentration resulted in the lowest fractions of multiply-occupied nanoholes
17
18 (see figure 4). Increasing the incubation time in 1x TAE was found to result in a continuous
19
20 decrease in the fraction of empty nanoholes from about 75 % after 1 h incubation to about 40 %
21
22 after 12 h (see figure 5). At the same time, the fraction of singly-occupied nanoholes increases
23
24 from about 20 % to about 50 %. Remarkably, the fraction of multiply-occupied nanoholes
25
26 increases only marginally with incubation time and reaches roughly 10 % after 12 h incubation.
27
28
29

30
31 A higher buffer strength of 2.5x again results in drastically different behavior. Here, the fraction
32
33 of singly-occupied nanoholes is steadily decreasing with incubation time, from about 30 % after
34
35 1 h to almost 0 % already after 3 h of incubation. This decrease is due to a dramatic increase in
36
37 the number of adsorbed DNA origami triangles per nanohole. After 3 h of incubation, the
38
39 majority of nanoholes, *i.e.* around 50 %, is occupied already by three DNA origami, while more
40
41 than 40 % of the nanoholes exhibit two DNA origami triangles. After 12 h of incubation,
42
43
44
45
46
47
48
49
50
51
52
53
54
55
56
57
58
59
60
virtually all the nanoholes are occupied by three or more DNA origami nanostructures.

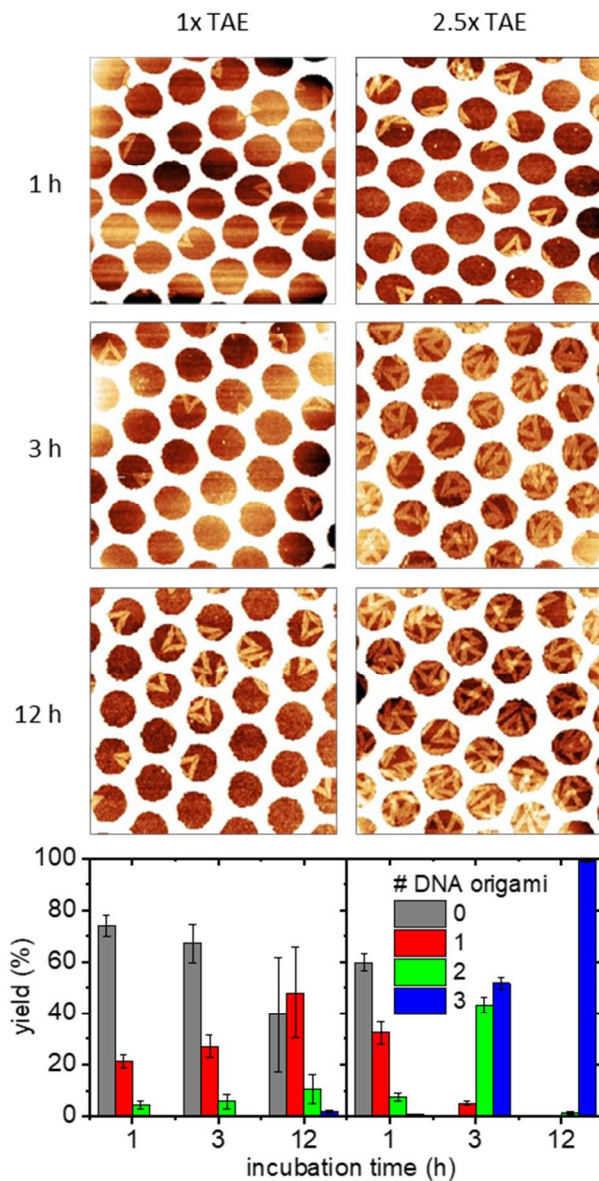


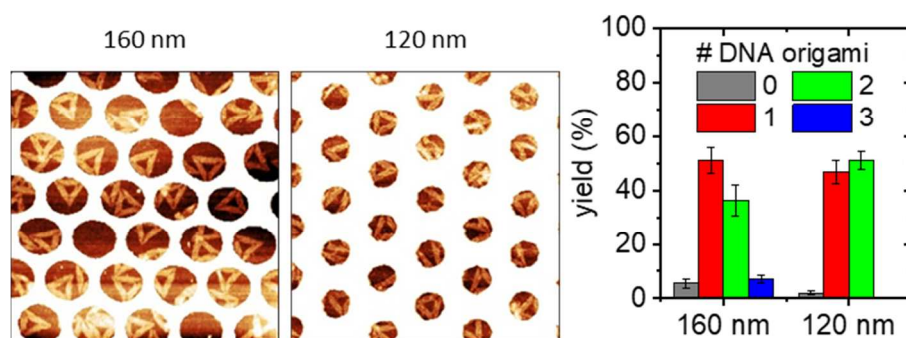
Figure 5. AFM images ($1 \times 1 \mu\text{m}^2$, height scales 3 nm) and corresponding statistical analyses of DNA origami triangles adsorbed in the nanohole arrays for two buffer strengths and three incubation times. The MgCl_2 and DNA origami concentration was 10 mM and 1 nM, respectively.

Above results demonstrate the tremendous importance of buffer strength in DNA origami adsorption in general and directed adsorption in particular. Based on these data, it appears

1
2
3 possible to obtain a yield of nanoholes occupied by only a single DNA origami triangle of more
4 than 50 %, in particular by using low buffer strengths, low Mg^{2+} concentrations, low DNA
5 origami concentrations, and long incubation times of 12 h and more. However, even under
6 optimized conditions, many of the single DNA origami nanostructures are not fully located
7 inside the nanoholes but rather cross the boundary to the Au film (see figures 3 and 5). This
8 partial DNA origami adsorption may result from two different effects. A low lateral mobility of
9 the adsorbed DNA origami nanostructures at the SiO_2 surface may prevent them from
10 maximizing their contact area with the oxide surface and thereby centering themselves in the
11 nanoholes. On the other hand, DNA origami may also adsorb to the surface of the Au film which
12 – in the case of comparable affinities for Au and SiO_2 – would result in random adsorption
13 instead of directed immobilization.
14
15
16
17
18
19
20
21
22
23
24
25
26
27
28

29 If low surface mobility of the DNA origami on the SiO_2 surface was responsible for the observed
30 partial adsorption in the nanoholes, reducing the diameter of the nanoholes to approach the size
31 of the DNA origami should lead to higher yields of singly-occupied nanoholes due to stronger
32 lateral confinement. Therefore, we have prolonged the plasma exposure of the assembled
33 nanospheres to reduce their diameter to 120 nm so that it matches the size of the DNA origami
34 triangles (see figure S3). Figure 6 shows AFM images and the corresponding statistical analyses
35 of DNA origami triangles adsorbed in the nanohole patterns with 120 nm and 160 nm diameter.
36 The adsorption conditions were chosen to result in a yield of about 50 % singly-occupied and
37 50 % multiply-occupied nanoholes with 160 nm diameter (see figure 4). As can be seen in figure
38 6, very similar distributions are obtained for both nanohole sizes. The only visible difference
39 between the statistical distributions in figure 6 is the apparent lack of 120 nm nanoholes
40 occupied by three DNA origami triangles. This may be a result of the small nanohole size that
41
42
43
44
45
46
47
48
49
50
51
52
53
54
55
56
57
58
59
60

1
2
3 even in the case of partial adsorption cannot accommodate more than two DNA origami
4 triangles. On the other hand, the small nanohole diameter makes identification of individual
5 DNA origami nanostructures inside the nanoholes quite difficult and may thus introduce a bias in
6 the statistical evaluation shown in figure 6. Nevertheless, these results demonstrate that partial
7 adsorption of DNA origami nanostructures cannot be significantly reduced by using smaller
8 nanohole diameters, thus hinting at the relevance of parasitic adsorption to the surface of the Au
9 film.
10
11
12
13
14
15
16
17
18
19



20
21
22
23
24
25
26
27
28
29
30
31
32 **Figure 6.** AFM images ($1 \times 1 \mu\text{m}^2$, height scales 3 nm) and corresponding statistical analyses of
33 DNA origami triangles adsorbed in a 160 nm nanohole array and a 120 nm nanohole array.
34 Adsorption conditions were 2.5 nM DNA origami in 2.5x TAE with 10 mM MgCl_2 for 1 h.
35
36
37
38

39 Due to the comparatively high roughness of the deposited Au film, we are unable to identify
40 DNA origami triangles crossing from the bottoms of the nanoholes to the surface of the Au film
41 in the AFM images (see figure S4). On smoother template-stripped Au surfaces, however, a
42 significant amount of adsorbed DNA origami can be detected even at low DNA origami and
43 MgCl_2 concentrations (see figure S5). This indeed suggests that parasitic DNA origami
44 adsorption to the surface of the Au film interferes with directing adsorption to the bottoms of the
45 nanoholes. Therefore, we have modified the surfaces of the Au films of 160 nm nanohole arrays
46 with a hydrophobic, CH_3 -terminated thiol SAM in order to minimize non-specific DNA origami
47
48
49
50
51
52
53
54
55
56
57
58
59
60

1
2
3 adsorption. The effect of this SAM has been evaluated for selected conditions which in the
4 previous experiments resulted in high DNA origami coverage (figure 7). Indeed, for all
5
6 previous experiments resulted in high DNA origami coverage (figure 7). Indeed, for all
7
8 conditions evaluated, application of the hydrophobic SAM resulted in significantly reduced DNA
9
10 origami adsorption. This clearly demonstrates the strong influence of non-specific adsorption to
11
12 the Au film. However, at low incubation times, the reduced overall adsorption results in a major
13
14 fraction of the nanoholes remaining empty, while long incubation times lead to distributions with
15
16 significant, albeit drastically reduced fractions of multiply occupied nanoholes. The latter seems
17
18 to be a direct result of the fact that many DNA origami are still not fully located inside the
19
20 nanoholes but cross the boundary to the Au film. Since non-specific DNA origami adsorption to
21
22 the gold film is blocked by the hydrophobic SAM, these observations can only be explained by
23
24 the low lateral mobility of the adsorbed DNA origami nanostructures at the SiO₂ surface. These
25
26 results thus proof that both effects, low surface mobility on the SiO₂ surface and parasitic
27
28 adsorption to the Au surface, negatively affect adsorption specificity.
29
30
31

32 33 **CONCLUSION**

34
35
36 The here presented study has identified several key parameters for optimizing adsorption
37
38 specificity of DNA origami nanostructures in nanohole arrays on SiO₂ surfaces. In particular,
39
40 comparatively high yields of nanoholes occupied by single DNA origami may be obtained for
41
42 low DNA origami and MgCl₂ concentrations of about 1 nM and 10 mM, respectively, low buffer
43
44 strength, and long incubation times exceeding 12 h. Furthermore, the strength of the adsorption
45
46 buffer was found to have a surprisingly strong influence on directed DNA origami adsorption
47
48 and may drastically alter the dependencies on the other parameters. However, even under
49
50 optimized conditions, many of the adsorbed DNA origami are not located completely inside the
51
52 nanoholes but rather cross the boundary to the surrounding Au film. This partial DNA origami
53
54
55
56
57
58
59
60

adsorption can be attributed to parasitic adsorption of DNA origami to the surface of the Au film and the low surface mobility of adsorbed DNA origami on the SiO₂ surface which prevents them from maximizing their contact area with the oxide surface.

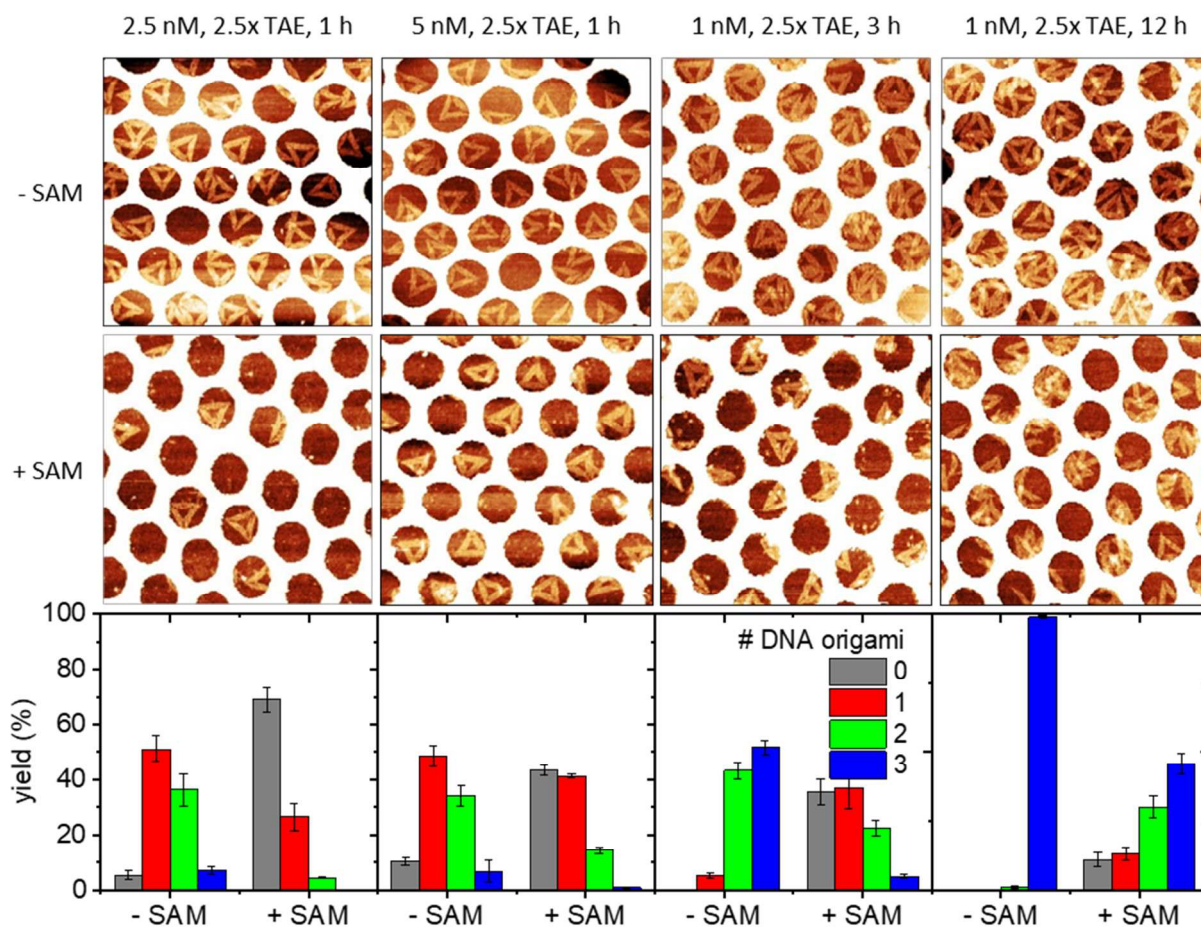


Figure 7. AFM images ($1 \times 1 \mu\text{m}^2$, height scales 3 nm) and corresponding statistical analyses of DNA origami triangles adsorbed under different conditions in 160 nm nanohole arrays with (+ SAM) and without (- SAM) application of a hydrophobic thiol SAM. DNA origami concentrations, buffer strengths, and incubation times are given in the figure.

While we have shown that parasitic adsorption to the Au film can be minimized by application of a hydrophobic thiol SAM, the problem of reduced lateral mobility could not be solved so far and may be affected by a number of parameters. In the present work, we have focused on TAE buffer

1
2
3 supplemented with MgCl_2 since this is probably the most widely used buffer in DNA origami
4 assembly. However, alternative buffer compositions may result in higher lateral mobility of once
5 adsorbed DNA origami nanostructures and thus improved localization accuracy. It was for
6 instance shown that addition of high concentrations of Na^+ ions may increase the lateral mobility
7 of DNA origami nanostructures on mica due to a partial replacement of Mg^{2+} ions from the mica
8 surface which results in a reduced positive surface charge and thus weaker electrostatic
9 interactions with the negatively charged DNA origami.^{16,51} Similarly, DNA binding to mica
10 surfaces may also be adjusted by using different divalent cations.⁵² The case of DNA origami
11 adsorption to SiO_2 surfaces, however, is more complicated. In particular, charge inversion of the
12 SiO_2 surface due to adsorption of divalent cations such as Mg^{2+} and Ca^{2+} occurs at much higher
13 cation concentrations (300 to 400 mM) than used in the present work.⁵³ Since charge inversion of
14 DNA in solution requires even higher Mg^{2+} concentrations,⁵⁴ DNA origami adsorption under the
15 current experimental conditions is likely facilitated by specific Mg^{2+} salt bridges forming
16 between the terminating silanol groups of the SiO_2 surface and the phosphates in the DNA
17 backbone.²⁹ In this case, using other divalent cations may result in very different and so far
18 unexplored DNA origami binding behaviors. The charge of the SiO_2 surface, the adsorption of
19 cations, and the formation of Mg^{2+} salt bridges furthermore depend on the protonation state of
20 the terminating silanol groups and thus on pH.⁵⁵ Adjustment of the pH of the adsorption buffer
21 may therefore represent another viable route toward optimizing localization accuracy. All these
22 issues deserve in-depth investigation in future studies.

23
24
25
26
27
28
29
30
31
32
33
34
35
36
37
38
39
40
41
42
43
44
45
46
47
48
49
50
51
52
53
54
55
56
57
58
59
60
Surface mobility of the DNA origami nanostructures may also be affected by the fabrication
process of the nanoholes and especially the different plasma treatment steps, as it is well known
that the surface energy of SiO_2 crucially depends on the nature and history of the specimens.⁵⁶

1
2
3 Furthermore, since most nanohole array sensors require optical access to both interfaces of the
4 metal film,⁴⁵ other transparent substrates such as the multitude of optical glasses but also
5 sapphire or indium tin oxide are worth investigating with regard to DNA origami adsorption and
6
7 may provide higher localization accuracy.
8
9

10
11
12 As an alternative strategy, the DNA origami design may be tailored with regard to the nanohole
13 dimension and geometry. For the circular nanoholes used in the present study, a disk-shaped
14 DNA origami with the same diameter as the nanoholes may occupy the whole surface area
15 available at the bottom and thus be able to block or at least reduce partial adsorption of other
16 DNA origami disks in the same nanohole. However, due to the limited scalability of DNA
17 origami size, this approach will be restricted to a rather narrow range of nanohole diameters.
18 Since single-layer DNA origami nanostructures other than the triangles used here are typically
19 rather floppy and show a certain tendency to rolling up,⁵⁷ stiffer multilayer DNA origami are
20 most likely more efficient in avoiding partial adsorption. This, however, will restrict the
21 accessible size range even further.
22
23
24
25
26
27
28
29
30
31
32
33
34
35

36 Finally, the nanohole arrays employed in above studies feature a rather thin Au film of 10 to 12
37 nm thickness (see figure 2e) in order to facilitate imaging of the bottoms of the nanoholes by
38 AFM. For most plasmonics-based sensing applications, however, films with thicknesses of the
39 order of 100 nm are required.⁴⁵ For such nanohole arrays, diffusion of the comparatively large
40 DNA origami nanostructures through the narrow nanochannels will affect adsorption kinetics
41 and become more and more dominant the closer the nanohole diameter approaches the size of the
42 DNA origami.⁵⁸ On the other hand, higher sidewalls may also more efficiently confine the DNA
43 origami to the exposed SiO₂ surface and thus further reduce the occurrence of partial DNA
44 origami adsorption, especially for mechanically rigid DNA origami designs.
45
46
47
48
49
50
51
52
53
54
55
56
57
58
59
60

ASSOCIATED CONTENT

Supporting Information: Comparison of cleaning procedures; optical characterization of the nanohole arrays by ellipsometry; SEM images of a monolayer of nanospheres shrunk to 120 nm diameter and the resulting nanohole array; additional AFM images of the 160 nm nanohole array after adsorption of 1 nM DNA origami in 1x TAE with 50 mM MgCl₂; AFM image of a template-stripped Au surface after DNA origami incubation.

AUTHOR INFORMATION

Corresponding Author

adrian.keller@uni-paderborn.de

Author Contributions

The manuscript was written through contributions of all authors. All authors have given approval to the final version of the manuscript. # These authors contributed equally.

Notes

The authors declare no competing financial interest.

ACKNOWLEDGMENT

We thank B. Mosebach and R. Hajiraissi for help with the fabrication of the template-stripped Au surfaces and the SAMs, respectively, and Y. Yang and T. de los Arcos for the ellipsometry characterization of the nanohole arrays.

REFERENCES

1
2
3 (1) Rothemund, P. W. K. Folding DNA to Create Nanoscale Shapes and Patterns. *Nature* **2006**,
4
5 *440*, 297–302.

6
7 (2) Nummelin, S.; Kommeri, J.; Kostianen, M. A.; Linko, V. Evolution of Structural DNA
8
9 Nanotechnology. *Adv. Mater.* **2018**, DOI: 10.1002/adma.201703721.

10
11 (3) Voigt, N. V.; Tørring, T.; Rotaru, A.; Jacobsen, M. F.; Ravnsbaek, J. B.; Subramani, R.;
12
13 Mamdouh, W.; Kjems, J.; Mokhir, A.; Besenbacher, F. *et al.* Single-molecule chemical reactions
14
15 on DNA origami. *Nat. Nanotechnol.* **2010**, *5*, 200–203.

16
17 (4) Steinhauer, C.; Jungmann, R.; Sobey, T. L.; Simmel, F. C.; Tinnefeld, P. DNA origami as a
18
19 nanoscopic ruler for super-resolution microscopy. *Angew. Chem. Int. Ed. Engl.* **2009**, *48*, 8870–
20
21 8873.

22
23 (5) Sacca, B.; Meyer, R.; Erkelenz, M.; Kiko, K.; Arndt, A.; Schroeder, H.; Rabe, K. S.;
24
25 Niemeyer, C. M. Orthogonal Protein Decoration of DNA Origami. *Angew. Chem. Int. Ed. Engl.*
26
27 **2010**, *49*, 9378–9383.

28
29 (6) Olejko, L.; Cywinski, P. J.; Bald, I. Ion-selective formation of a guanine quadruplex on
30
31 DNA origami structures. *Angew. Chem. Int. Ed. Engl.* **2015**, *54*, 673–677.

32
33 (7) Sharma, J.; Chhabra, R.; Andersen, C. S.; Gothelf, K. V.; Yan, H.; Liu, Y. Toward reliable
34
35 gold nanoparticle patterning on self-assembled DNA nanoscaffold. *J. Am. Chem. Soc.* **2008**, *130*,
36
37 7820–7821.

38
39 (8) Ko, S. H.; Gallatin, G. M.; Liddle, J. A. Nanomanufacturing with DNA Origami: Factors
40
41 Affecting the Kinetics and Yield of Quantum Dot Binding. *Adv. Funct. Mater.* **2012**, *22*, 1015–
42
43 1023.

44
45 (9) Raz, M. H.; Hidaka, K.; Sturla, S. J.; Sugiyama, H.; Endo, M. Torsional Constraints of DNA
46
47 Substrates Impact Cas9 Cleavage. *J. Am. Chem. Soc.* **2016**, *138*, 13842–13845.
48
49
50
51
52
53
54
55
56
57
58
59
60

1
2
3 (10) Zhao, Y.-X.; Shaw, A.; Zeng, X.; Benson, E.; Nystrom, A. M.; Hogberg, B. DNA origami
4 delivery system for cancer therapy with tunable release properties. *ACS Nano* **2012**, *6*, 8684–
5 8691.
6
7

8
9
10 (11) Ora, A.; Jarvihaavisto, E.; Zhang, H.; Auvinen, H.; Santos, H. A.; Kostianen, M. A.;
11 Linko, V. Cellular delivery of enzyme-loaded DNA origami. *Chem. Commun.* **2016**, *52*, 14161–
12 14164.
13
14

15
16 (12) Ke, Y.; Lindsay, S.; Chang, Y.; Liu, Y.; Yan, H. Self-assembled water-soluble nucleic acid
17 probe tiles for label-free RNA hybridization assays. *Science* **2008**, *319*, 180–183.
18
19

20
21 (13) Walter, H.-K.; Bauer, J.; Steinmeyer, J.; Kuzuya, A.; Niemeyer, C. M.; Wagenknecht, H.-
22 A. "DNA Origami Traffic Lights" with a Split Aptamer Sensor for a Bicolor Fluorescence
23 Readout. *Nano Lett.* **2017**, *17*, 2467–2472.
24
25

26
27 (14) Prinz, J.; Schreiber, B.; Olejko, L.; Oertel, J.; Rackwitz, J.; Keller, A.; Bald, I. DNA
28 Origami Substrates for Highly Sensitive Surface-Enhanced Raman Scattering. *J. Phys. Chem.*
29 *Lett.* **2013**, *4*, 4140–4145.
30
31

32
33 (15) Simoncelli, S.; Roller, E.-M.; Urban, P.; Schreiber, R.; Turberfield, A. J.; Liedl, T.;
34 Lohmüller, T. Quantitative Single-Molecule Surface-Enhanced Raman Scattering by
35 Optothermal Tuning of DNA Origami-Assembled Plasmonic Nanoantennas. *ACS Nano* **2016**,
36 *10*, 9809–9815.
37
38

39
40 (16) Ramakrishnan, S.; Subramaniam, S.; Stewart, A. F.; Grundmeier, G.; Keller, A. Regular
41 Nanoscale Protein Patterns via Directed Adsorption through Self-Assembled DNA Origami
42 Masks. *ACS Appl. Mater. Interfaces* **2016**, *8*, 31239–31247.
43
44

45
46 (17) Surwade, S. P.; Zhao, S.; Liu, H. Molecular Lithography Through DNA-Mediated Etching
47 and Masking of SiO₂. *J. Am. Chem. Soc.* **2011**, *133*, 11868–11871.
48
49
50

- 1
2
3 (18) Geng, Y.; Pearson, A. C.; Gates, E. P.; Uprety, B.; Davis, R. C.; Harb, J. N.; Woolley, A. T.
4 Electrically conductive gold- and copper-metallized DNA origami nanostructures. *Langmuir*
5
6 **2013**, *29*, 3482–3490.
7
8
9
10 (19) Teschome, B.; Facsko, S.; Schonherr, T.; Kerbusch, J.; Keller, A.; Erbe, A. Temperature-
11
12 Dependent Charge Transport through Individually Contacted DNA Origami-Based Au
13
14 Nanowires. *Langmuir* **2016**, *32*, 10159–10165.
15
16
17 (20) Klein, W. P.; Schmidt, C. N.; Rapp, B.; Takabayashi, S.; Knowlton, W. B.; Lee, J.; Yurke,
18
19 B.; Hughes, W. L.; Graugnard, E.; Kuang, W. Multiscaffold DNA origami nanoparticle
20
21 waveguides. *Nano Lett.* **2013**, *13*, 3850–3856.
22
23
24 (21) Shen, B.; Linko, V.; Tapio, K.; Pikker, S.; Lemma, T.; Gopinath, A.; Gothelf, K. V.;
25
26 Kostiainen, M. A.; Toppari, J. J. Plasmonic nanostructures through DNA-assisted lithography.
27
28 *Sci. Adv.* **2018**, *4*, eaap8978.
29
30
31 (22) Olejko, L.; Cywiński, P. J.; Bald, I. An ion-controlled four-color fluorescent telomeric
32
33 switch on DNA origami structures. *Nanoscale* **2016**, *8*, 10339–10347.
34
35
36 (23) Stein, I. H.; Steinhauer, C.; Tinnefeld, P. Single-molecule four-color FRET visualizes
37
38 energy-transfer paths on DNA origami. *J. Am. Chem. Soc.* **2011**, *133*, 4193–4195.
39
40
41 (24) Ding, B.; Wu, H.; Xu, W.; Zhao, Z.; Liu, Y.; Yu, H.; Yan, H. Interconnecting gold islands
42
43 with DNA origami nanotubes. *Nano Lett.* **2010**, *10*, 5065–5069.
44
45
46 (25) Gao, B.; Sarveswaran, K.; Bernstein, G. H.; Lieberman, M. Guided deposition of individual
47
48 DNA nanostructures on silicon substrates. *Langmuir* **2010**, *26*, 12680–12683.
49
50
51 (26) Gerdon, A. E.; Oh, S. S.; Hsieh, K.; Ke, Y.; Yan, H.; Soh, H. T. Controlled delivery of
52
53 DNA origami on patterned surfaces. *Small* **2009**, *5*, 1942–1946.
54
55
56
57
58
59
60

1
2
3 (27) Gopinath, A.; Miyazono, E.; Faraon, A.; Rothmund, P. W. K. Engineering and mapping
4 nanocavity emission via precision placement of DNA origami. *Nature* **2016**, *535*, 401–405.

5
6
7 (28) Gopinath, A.; Rothmund, P. W. K. Optimized assembly and covalent coupling of single-
8 molecule DNA origami nanoarrays. *ACS Nano* **2014**, *8*, 12030–12040.

9
10
11 (29) Kershner, R. J.; Bozano, L. D.; Micheel, C. M.; Hung, A. M.; Fornof, A. R.; Cha, J. N.;
12 Rettner, C. T.; Bersani, M.; Frommer, J.; Rothmund, P. W. K. *et al.* Placement and orientation
13 of individual DNA shapes on lithographically patterned surfaces. *Nat. Nanotechnol.* **2009**, *4*,
14 557–561.

15
16
17 (30) Yun, J. M.; Kim, K. N.; Kim, J. Y.; Shin, D. O.; Lee, W. J.; Lee, S. H.; Lieberman, M.;
18 Kim, S. O. DNA origami nanopatterning on chemically modified graphene. *Angew. Chem. Int.*
19 *Ed. Engl.* **2012**, *51*, 912–915.

20
21
22 (31) Kopielski, A.; Csaki, A.; Fritzsche, W. Surface Mobility and Ordered Rearrangement of
23 Immobilized DNA Origami. *Langmuir* **2015**, *31*, 12106–12110.

24
25
26 (32) Teschome, B.; Facsko, S.; Gothelf, K. V.; Keller, A. Alignment of Gold Nanoparticle-
27 Decorated DNA Origami Nanotubes: Substrate Pre patterning versus Molecular Combing.
28 *Langmuir* **2015**, *31*, 12823–12829.

29
30
31 (33) Teshome, B.; Facsko, S.; Keller, A. Topography-controlled alignment of DNA origami
32 nanotubes on nanopatterned surfaces. *Nanoscale* **2014**, *6*, 1790–1796.

33
34
35 (34) Pearson, A. C.; Pound, E.; Woolley, A. T.; Linford, M. R.; Harb, J. N.; Davis, R. C.
36 Chemical alignment of DNA origami to block copolymer patterned arrays of 5 nm gold
37 nanoparticles. *Nano Lett.* **2011**, *11*, 1981–1987.

38
39
40 (35) Hulteen, J. C.; van Duyne, R. P. Nanosphere lithography: A materials general fabrication
41 process for periodic particle array surfaces. *J. Vac. Sci. Technol. A* **1995**, *13*, 1553–1558.

1
2
3 (36) Dimitrov, A. S.; Nagayama, K. Continuous Convective Assembling of Fine Particles into
4 Two-Dimensional Arrays on Solid Surfaces. *Langmuir* **1996**, *12*, 1303–1311.

7 (37) Born, P.; Blum, S.; Munoz, A.; Kraus, T. Role of the meniscus shape in large-area
8 convective particle assembly. *Langmuir* **2011**, *27*, 8621–8633.

11 (38) Fredriksson, H.; Alaverdyan, Y.; Dmitriev, A.; Langhammer, C.; Sutherland, D. S.; Zäch,
12 M.; Kasemo, B. Hole–Mask Colloidal Lithography. *Adv. Mater.* **2007**, *19*, 4297–4302.

15 (39) Singh, G.; Gohri, V.; Pillai, S.; Arpanaei, A.; Foss, M.; Kingshott, P. Large-area protein
16 patterns generated by ordered binary colloidal assemblies as templates. *ACS Nano* **2011**, *5*,
17 3542–3551.

20 (40) Agheli, H.; Malmström, J.; Larsson, E. M.; Textor, M.; Sutherland, D. S. Large area protein
21 nanopatterning for biological applications. *Nano Lett.* **2006**, *6*, 1165–1171.

24 (41) Ogaki, R.; Bennetsen, D. T.; Bald, I.; Foss, M. Dopamine-assisted rapid fabrication of
25 nanoscale protein arrays by colloidal lithography. *Langmuir* **2012**, *28*, 8594–8599.

28 (42) Coe, J. V.; Heer, J. M.; Teeters-Kennedy, S.; Tian, H.; Rodriguez, K. R. Extraordinary
29 transmission of metal films with arrays of subwavelength holes. *Annu. Rev. Phys. Chem.* **2008**,
30 *59*, 179–202.

33 (43) Genet, C.; Ebbesen, T. W. Light in tiny holes. *Nature* **2007**, *445*, 39–46.

36 (44) Masson, J.-F.; Murray-Méthot, M.-P.; Live, L. S. Nanohole arrays in chemical analysis:
37 Manufacturing methods and applications. *Analyst* **2010**, *135*, 1483–1489.

40 (45) Escobedo, C. On-chip nanohole array based sensing: A review. *Lab Chip* **2013**, *13*, 2445–
41 2463.

1
2
3 (46) Pibiri, E.; Holzmeister, P.; Lalkens, B.; Acuna, G. P.; Tinnefeld, P. Single-molecule
4 positioning in zeromode waveguides by DNA origami nanoadapters. *Nano Lett.* **2014**, *14*, 3499–
5 3503.
6
7

8
9
10 (47) Rüdiger, A. A.; Brassat, K.; Lindner, J. K. N.; Bremser, W.; Strube, O. I. Easily Accessible
11 Protein Nanostructures via Enzyme Mediated Addressing. *Langmuir* **2018**, *34*, 4264–4270.
12

13
14 (48) Gogel, D.; Weini, M.; Lindner, J.; Stritzker, B. Plasma modification of nanosphere
15 lithography masks made of polystyrene beads. *J. Optoelectron. Adv. Mater.* **2010**, *12*.
16

17
18 (49) Hajiraissi, R.; Hanke, M.; Yang, Y.; Duderija, B.; Gonzalez Orive, A.; Grundmeier, G.;
19 Keller, A. Adsorption and fibrillization of islet amyloid polypeptide at self-assembled
20 monolayers studied by QCM-D, AFM, and PM-IRRAS. *Langmuir* **2018**, DOI:
21 10.1021/acs.langmuir.7b03626.
22
23
24
25

26
27 (50) Brassat, K.; Assion, F.; Hilleringmann, U.; Lindner, J. K. N. Self-organization of
28 nanospheres in trenches on silicon surfaces. *Phys. Status Solidi A* **2013**, *210*, 1485–1489.
29
30

31
32 (51) Aghebat Rafat, A.; Pirzer, T.; Scheible, M. B.; Kostina, A.; Simmel, F. C. Surface-Assisted
33 Large-Scale Ordering of DNA Origami Tiles. *Angew. Chem. Int. Ed. Engl.* **2014**, *53*, 7665–7668.
34
35

36
37 (52) Hansma, H. G.; Laney, D. E. DNA binding to mica correlates with cationic radius: Assay
38 by atomic force microscopy. *Biophys. J.* **1996**, *70*, 1933–1939.
39
40

41
42 (53) van der Heyden, F. H. J.; Stein, D.; Besteman, K.; Lemay, S. G.; Dekker, C. Charge
43 inversion at high ionic strength studied by streaming currents. *Phys. Rev. Lett.* **2006**, *96*, 224502.
44
45

46
47 (54) Pastré, D.; Hamon, L.; Landousy, F.; Sorel, I.; David, M.-O.; Zozime, A.; Le Cam, E.;
48 Piétrement, O. Anionic polyelectrolyte adsorption on mica mediated by multivalent cations: A
49 solution to DNA imaging by atomic force microscopy under high ionic strengths. *Langmuir*
50 **2006**, *22*, 6651–6660.
51
52
53
54
55

1
2
3 (55) Dove, P. M.; Craven, C. M. Surface charge density on silica in alkali and alkaline earth
4 chloride electrolyte solutions. *Geochim. Cosmochim. Acta* **2005**, *69*, 4963–4970.

5
6
7 (56) Keller, A.; Facsko, S.; Möller, W. Evolution of ion-induced ripple patterns on SiO₂
8 surfaces. *Nucl. Instrum. Methods Phys. Res., Sect. B* **2009**, *267*, 656–659.

9
10
11 (57) Li, Z.; Wang, L.; Yan, H.; Liu, Y. Effect of DNA hairpin loops on the twist of planar DNA
12 origami tiles. *Langmuir* **2012**, *28*, 1959–1965.

13
14
15 (58) Martin, F.; Walczak, R.; Boiarski, A.; Cohen, M.; West, T.; Cosentino, C.; Shapiro, J.;
16 Ferrari, M. Tailoring width of microfabricated nanochannels to solute size can be used to control
17 diffusion kinetics. *J. Control. Release* **2005**, *102*, 123–133.
18
19
20
21
22
23
24
25
26
27
28
29
30
31
32
33
34
35
36
37
38
39
40
41
42
43
44
45
46
47
48
49
50
51
52
53
54
55
56
57
58
59
60

1
2
3 **TABLE OF CONTENTS GRAPHIC**
4
5

